Physica E 154 (2023) 115812

Contents lists available at ScienceDirect

Physica E: Low-dimensional Systems and Nanostructures

journal homepage: www.elsevier.com/locate/physe

Tensile strain creates trion: Excitonic photoluminescence distribution over bilayer MoS_2 grown by CVD

Oleksandr I. Datsenko [a], Sergii Golovynskyi [b,*], Ana I. Pérez-Jiménez [c], Marc Chaigneau [d], Andrii Golovynskyi [e], Iuliia Golovynska [b], Victoriya Shevchenko [a], Matteo Bosi [f], Luca Seravalli [f]

[a] Physics Department, Taras Shevchenko National University of Kyiv, 01601, Kyiv, Ukraine
[b] College of Physics and Optoelectronic Engineering, Shenzhen University, 518060, Shenzhen, PR China
[c] Technology Innovation Institute, 9639, Masdar City, Abu Dhabi, United Arab Emirates
[d] Horiba Scientific, 91120, Palaiseau, France
[e] V.M. Glushkov Institute of Cybernetics, National Academy of Sciences, Kyiv, 03187, Ukraine
[f] Institute of Materials for Electronics and Magnetism, IMEM-CNR, I-43124, Parma, Italy

ARTICLE INFO

Keywords:
Molybdenum disulfide
Photoluminescence
Exciton
Trion
Strain

ABSTRACT

Raman and photoluminescence (PL) hyperspectral mapping of a bilayer MoS_2 flake grown on SiO_2/Si substrate by chemical vapor deposition is studied focusing on the surface variation of the exciton and trion PL characteristics. The Raman modes and the excitonic PL in the flake interior are redshifted compared to those at the perimeter. This is attributed to tensile strain present after the post-growth cooling so that the flake perimeter is less strained. At the perimeter, the PL blueshift is also enhanced due to a reduction of the trion (a negatively charged exciton) peak, being attributed to an outflow of electrons (*p*-doping) induced by a weakening of tensile strain towards the flake edge. This occurs because tensile strain bends down the conduction band of MoS_2, causing a drift of electrons towards the strained interior region and, in turn, creating there an increased electron density which fosters the creation of trion.

1. Introduction

Two-dimensional (2D) transition metal dichalcogenides are novel promising materials for optoelectronics, which gained a tremendous scientific interest in recent years. Having indirect bandgap in bulk, they acquire direct one when becoming monolayer (1L) [1–4]. Among them, molybdenum disulfide (MoS_2) is one of the most investigated. Only 1L MoS_2 flakes manifest high luminescence efficiency, related to the emission of exciton and trion (a negatively charged three-particle exciton-like creation with an additional electron) [5–7]. However, the reabsorption in a few-layer flake is rather weak, thus emission from such flakes, although being several times less than the one from a 1L flake, remains acceptable for practical application. Moreover, the optical and luminescent properties may be modified by doping, by contact with metal [8–11], semiconductor [12–21] nanoparticles, and by the presence of strain [22–28].

Furthermore, the properties of 2D MoS_2 highly depend on the fabrication method and the substrate used. In particular, tensile strain is introduced into a flake during the cooling after growth by chemical vapor deposition (CVD) at high temperatures [29], as the thermal expansion coefficient of MoS_2 highly exceeds those of SiO_2 and Si [25,30,31]. As a result, tensile strain lowers the bandgap and increases the lattice constant. The strain leads to an inhomogeneous photoluminescence (PL) efficiency from different areas of the flake surface: the emission from the flake interior is redshifted compared to the one at the less strained perimeter. The effect of strain [22–28], including the one induced by the post-growth cooling [25,30–33], has been widely studied.

It has been suggested that, beside the strain, the properties of the edge itself can lead to an additional doping effect on the flake perimeter [32,34,35]: Bao et al. [33] noticed a contribution of the long-wavelength trion in the PL spectrum at the perimeter. This indicated an *n*-doping effect at the edge, resulting in a slight reduction of the strain-induced PL blueshift. The researchers attributed this phenomenon to the presence of a Mo-terminated edge, which introduces a *n*-doping at the edge.

Bao et al. [33] were the first to separate the trion component in the excitonic PL spectra derived across the surfaces of CVD-grown MoS_2

* Corresponding author.
E-mail address: serge@szu.edu.cn (S. Golovynskyi).

https://doi.org/10.1016/j.physe.2023.115812
Received 31 May 2023; Received in revised form 22 July 2023; Accepted 2 August 2023
Available online 2 August 2023
1386-9477/© 2023 Elsevier B.V. All rights reserved.

flakes among those who studied strains in MoS_2. So, the investigation of the strain effects on excitonic PL in CVD-grown flakes chiefly considered 1L MoS_2 with direct bandgap. However, there is an exception worth mentioning: our recent study [31] explored both the exciton and trion PL in low-strained bilayer (2L) MoS_2 flakes. Unfortunately, the spatial resolution of Raman/PL imaging was not sufficient to clearly investigate the strain effects. 2L MoS_2 is less investigated than its 1L counterpart. 1L MoS_2 exists at the 2D quantum limit for this material, with no interlayer interaction and reduced screening effect; conversely, electronic structure and indirect bandgap of 2L MoS_2 are defined by quantum confinement, interlayer interaction, screening effect and crystal symmetry [3,7,36]. As a result, the excitonic PL of 2L MoS_2 is about 2-times less intense than in 1L material [27,36,37]. However, 2L MoS_2 has a more prominent trion contribution, thus being a promising candidate for nano-optoelectronic application [38–41] and offering a unique platform to investigate the fundamental phenomena arising from the trion creation and exciton-trion interaction [31,36,37,42,43].

In this work, we study in detail the variation of the micro-Raman and micro-PL spectra across an edge of a 2L MoS_2 flake, using sub-micron imaging resolution. Particular attention is paid to the exciton and trion PL behavior upon the growth-induced tensile strain in the flakes. It is found that the perimeter of the flakes is less strained and has a blue-shifted PL due to the strain-induced variation of the bandgap. The strain-induced band bending towards the flake edge is analyzed considering the trion contribution.

2. Experiment

2D MoS_2 flakes were grown by CVD on the surface of a Si wafer covered by a 290 μm thick SiO_2 thermal oxide layer, using solid state precursors and following the method described in-detail in our previous reports [42,44,45].

Morphology and PL/Raman imaging were combined for the sample characterization on a sub-micron spatial resolution: an atomic force microscopy (AFM) image was obtained by means of a SmartSPM Horiba scanning probe microscope; PL and Raman micro-imaging and spectroscopies were carried out using a LabRam HR Evolution Horiba Raman/PL confocal microscope. Laser excitation was focused onto the sample surface to a ~400 nm diameter spot (~80 mW/μm^2) using an 100× objective. The PL mapping of the studied flake was obtained under 633 nm (1.96 eV) excitation with a spatial step of ~170 nm, the spectra before the analysis were recalculated to be proportional to the number of quanta per energy unit. For the Raman mapping, 532 nm excitation was used with a step of 400 nm. All the measurements were performed at room temperature.

3. Results

A single-crystal 2L MoS_2 flake has been chosen for the study. According to AFM (Fig. 1a), the flake has a triangular shape with a side length of ~17 μm, while the height profile over the flake area (see inset Fig. 1a) allows to estimate its thickness as ~1.5 nm. Taking into account the expected 1L MoS_2 thickness of 0.7–0.8 nm [2,5–7], this value corresponds to a 2L structure.

Under optical excitation, the flake demonstrates variable PL properties over the surface (Fig. 1b). The PL spectra at the flake perimeter and interior are given in Fig. 2a. One can see that the spectra under the 633 nm excitation are single bands, while the pronounced asymmetry of the band obtained in the interior evidences the presence of at least two components. Based on the known results [7,31,36,37,42], we can infer that the PL band is related to the A exciton (the A^0 component), while the long-wave shoulder is due to the negatively charged trion (the A^- component). As a rule, a weaker B exciton band is also observed at $\lesssim$ 620 nm, but it is not observable for our excitation at 633 nm.

According to the PL mapping of the peak intensity and peak position (Fig. 1b), the PL band redshifts when moving from the edge towards the interior, which is expected if considering a possible effect of tensile strain present in the flake on the SiO_2/Si substrate after the post-growth cooling. Additionally, the PL intensity near the edge is slightly higher than the intensity in the interior, as observed in some other similar studies of CVD-grown flakes [25,30–33].

Furthermore, the Raman spectra were studied under the excitation of 532 nm (Fig. 1c and d and 3a). The Raman spectra (Fig. 3a) reveal the modes E^1_{2g} (~385 cm^{-1}) and A_{1g} (~405 cm^{-1}) related, respectively, to in-plane and out-of-plane vibrations. The distance between these modes depends on the 2D flake thickness [46], and our value of ~20 cm^{-1} is an additional evidence of a 2L structure of the studied object [46,47].

The Raman mapping of these modes (Fig. 1c and d) shows a uniform intensity distribution over the flake surface, while the peak positions, similarly to the PL spectra (Fig. 1b), show a blue shift in the inner zone. This is also characteristic for strained CVD-grown flakes [25,30,31]. When analyzing the Raman spectra across the edge (along the white line on the mappings), the Raman peaks were fitted with Lorentzian functions (Fig. 3a). The extracted parameters are plotted in Fig. 3b. The

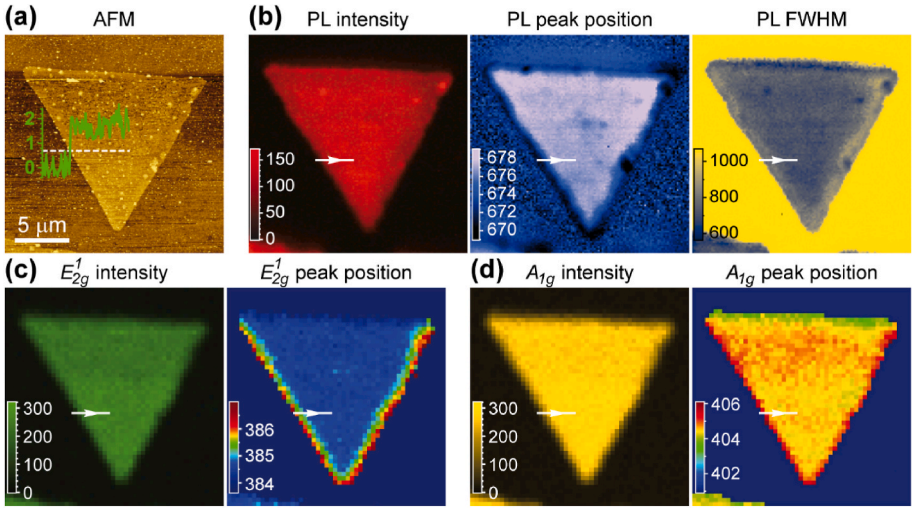

Fig. 1. Correlative characterization of morphology and PL/Raman of the 2L MoS_2 flake grown using CVD: (a) images of AFM, (b) PL peak intensity, position and width as well as the peak intensities and positions of the Raman modes E^1_{2g} (c) and A_{1g} (d). The intensity scales are in counts, the peak position and width scales of the PL and Raman bands are, respectively, in nm and cm^{-1}.

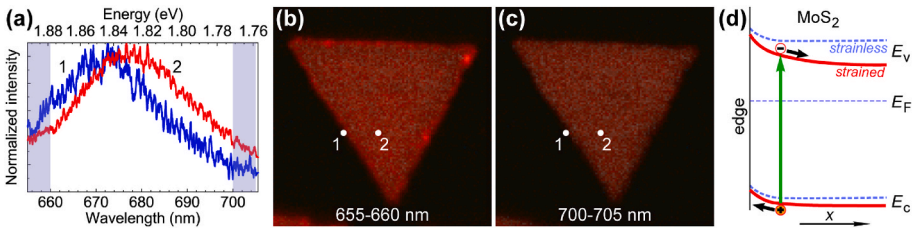

Fig. 2. (a) PL spectra of the 2L MoS_2 flake at the edge (curve 1) and interior (curve 2) under 633 nm excitation, the measurement points are marked at the images. (b,c) PL intensity mapping at the opposite ranges of the measured spectra, the gray areas showed in (a); the color scale is the same as at the respective image in Fig. 1b. (d) Schematic of the tensile-strain-related bending of energy bands near a flake edge and the induced drift of charge carriers leading to the trion formation in a strained area.

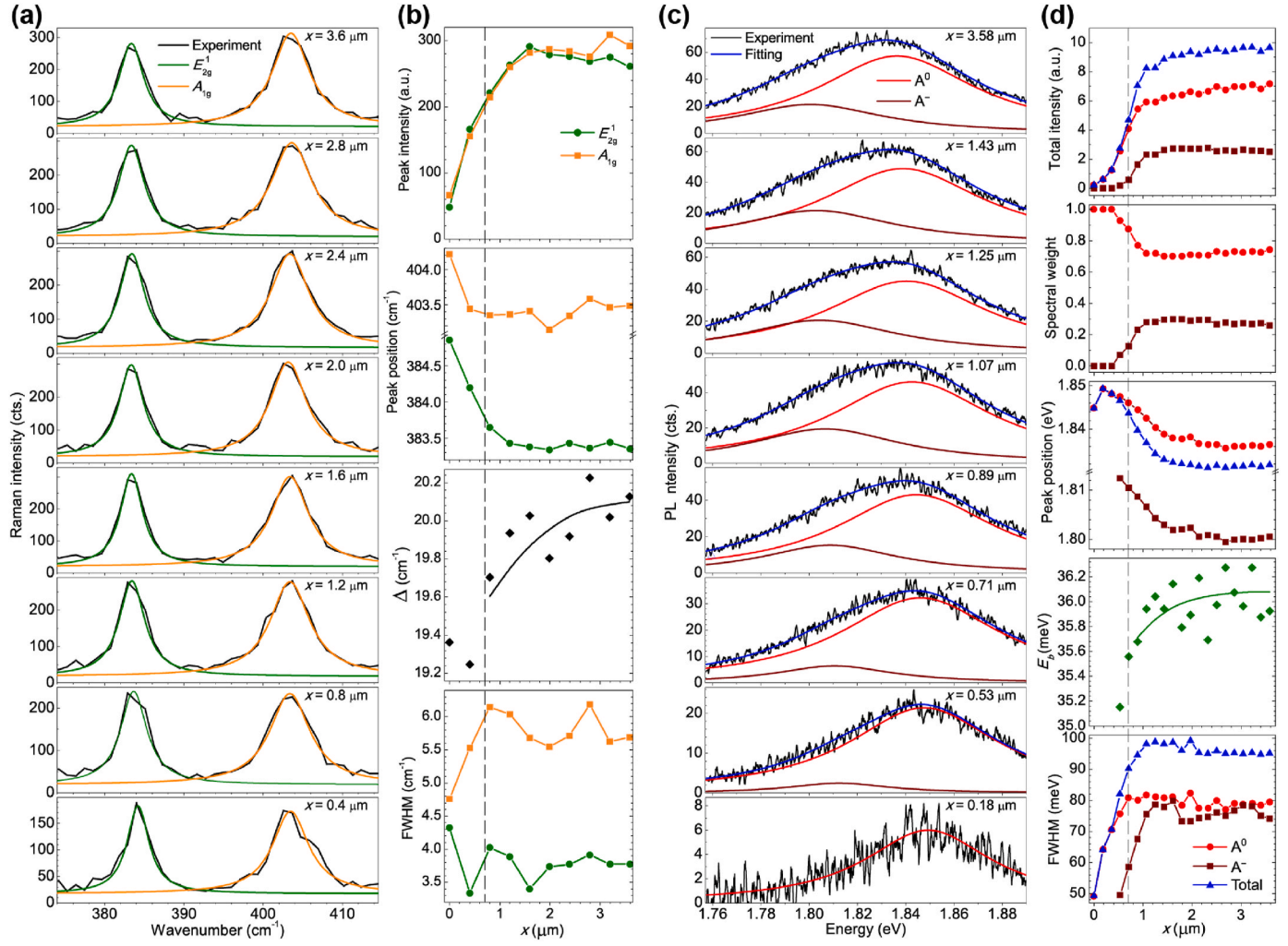

Fig. 3. Raman (a) and PL (c) spectra of the 2L MoS_2 flake along the white line at the images in Fig. 1b,c,d and their fitting with two Lorentzian functions. Plots of parameters of the bands fitting the Raman (b) and PL (d) spectra as well as the spectral weight of the PL bands, the distance between the Raman modes (Δ) and PL components (trion binding energy, E_b), the curves are guides for the eye. The vertical dashed lines across the plots mark the position of the flake edge. The coordinate $x = 0$ (beginning of the white line at the mappings near the edge of the flake) corresponds to the point where the PL band out of the flake is still detectable.

distance Δ between the modes increases when moving from the edge to the interior. This is in a complete agreement with the fact that the A_{1g} mode is less strain-dependent compared to the E^1_{2g} one [22–24,28], so that Δ should increase towards the strained interior. We can rule out the effect of a possible reduction of thickness at the perimeter on the basis of AFM data that indicate a 2L structure also at the flake edges.

The parameters of the exciton and trion components of the PL spectra vary in a different way over the flake surface (Fig. 1b). This is notable if comparing the PL spectra inside and at the perimeter of the flake (Fig. 2a). While the former is obviously distorted by the long-wave A^- component, the latter looks symmetrical relatively to the peak position, showing a dominant contribution of the A^0 exciton. This is more visible on the PL mapping if considering the opposite areas of the studied spectral range (the gray areas in Fig. 2a). Considering only the short-wave part in Fig. 2b, we can see a clear increase in the intensity at the perimeter, otherwise, involving only the long-wave part in Fig. 2c, the intensity decreases towards the edges. This may evidence a decrease of the trion contribution to the spectrum at the less strained perimeter. Respectively, a PL band narrowing is observed at the flake edges in Fig. 1b (the area of greatest FWHM deeper to the interior is perhaps related to the lower intensity and, hence, to the noise effect distorting the result, as it correlates with the intensity distribution on the mapping).

To check this assumption, the PL spectra measured across the edge

(along the white line at the mappings in Fig. 3b) were fitted using two Lorentzian functions (Fig. 3c), considering the A^0 and A^- peaks. The fitting parameters such as integral intensity, peak position and FWHM were plotted along the coordinate axis in Fig. 3d. Indeed, the trion contribution to the PL spectrum increases towards the interior, as shown in the plot of the spectral weight. According to the trion nature, the trion binding energy (E_b, the energy distance between the A^0 and A^- peaks) also gradually increases towards the interior (Fig. 3d). The obtained value is about 36 meV. Trion binding energy in MoS_2 is known to be much less than exciton binding energy, which is several hundreds of meV [48]. In particular, the experimentally obtained value of binding energy for exciton in bilayer MoS_2 is above 700 meV [49].

It is worthwhile noting that some points were analyzed in-detail even if they are located outside the flake (see the white line in the PL mappings). The point $x = 0$ was chosen in terms of an assured observation of the PL band, while the position of the edge is at $x \approx 0.7$ μm (it is marked in the plots by a dashed line), if carefully comparing the respective sizes on the AFM and Raman/PL images. Nevertheless, the PL is detected out of the flake even 0.7 μm from the edge, while the spot of laser excitation is only ~0.4 μm in diameter. We attribute this effect to the excitation and emission scattering by the ~300 μm thick SiO_2 substrate layer. Both Rayleigh and Mie scattering are known to be highly dependent on the wavelength or quantum energy, and this can explain an essential narrowing and notable redshift of the PL band outside the flake (see the peak position and FWHM plots). Thus, the information from the points to the left of the ~0.9 μm point (including ~0.2 μm of the laser spot radius) is distorted, and the respective points in Fig. 3 are reported only for the sake of consistency.

4. Discussion

The trion contribution decreases from the flake interior towards the edge, becoming indistinguishable at the perimeter. It is known that strain creates a trion [22,50,51]: tensile strain bends down the conduction band edge of MoS_2 [22,52–54], causing a drift of electrons towards the strained region and, in turn, creating there an increased electron density which fosters the creation of trion. Accordingly, the less strained flake perimeter should have an electron deficiency and a lower intensity of the trion component (schematically shown in Fig. 2d). We observe that the trion binding energy, E_b, reveals a trend to increase towards the interior. This is also in accordance with the strain effect causing an increased electron density, as other authors confirm a stronger shift of the A^- trion band compared to the A^0 exciton under tensile strain in 1L MoS_2 [28] and also WS_2 [50,51,55]. The increase in E_b can be attributed to the strain-related band bending and the subsequent increase in electron density (as depicted in the schematic in Fig. 2d). This effect is further supported by the fact that the energy distance between the exciton and trion increases with *n*-doping [7,9,36,37,56,57].

The strain effects are also confirmed by the blueshift towards the perimeter of both the A^0 and A^- components. Due to the heterogeneous tensile strain, the lattice parameter in the interior is elongated with respect to the one at the perimeter, affecting the band structure of the material and decreasing the bandgap. However, the shift of the total spectrum is notably stronger due to the variation of the A^- contribution. The reduction in the trion band causes a decrease in the FWHM of the overall spectrum band. However, the FWHM of the A^0 component remains unchanged, although there is a narrowing of the A^- band towards the edge. This narrowing could be attributed to the lower electron density near the edge and a narrowing of electron localization function at the virtual trion level.

Our results on the A^- trion contribution in different surface areas of the flake are in general agreement with the basic knowledge on the influence of heterogeneous tensile strain on the exciton and trion [22,28,50,51,55]. However, they are in some contradiction with the data obtained for 1L MoS_2 by Bao et al. [33], who observed an enhancement of the trion contribution to the PL at the perimeter, which, in turn, caused a broadening of the total PL band. It should be noted that, among all the works on CVD-growth-induced strain and edge effect in 1L MoS_2, only Bao et al. deconvoluted the studied spectra with the exciton and trion. Most articles did not analyze the spectral composition of the main A band, but some paid attention to the bandwidth, observing also an increase of FWHM at the flake perimeter [32]. Our recent study on CVD-grown 2L MoS_2 [31] also showed an increase in both the trion contribution and the total PL bandwidth at the edge of a flake compared to that in the interior, allowing to exclude an effect of the thickness.

As the trion is a negative exciton after capturing an additional electron, its formation highly depends on the material doping and, thus, on factors that affect the doping. They were preferentially studied for the 1L material with a direct bandgap, but a thicker indirect-gap MoS_2 was also investigated. It was found that the trion contribution to the PL spectrum of few-layer MoS_2 depends on temperature [29,42], excitation power and energy [37,58], and varies if coupled to nanoparticles used as PL sensitizers [10,11]. No direct effect of strains on the trion formation was studied on few-layer flakes, but it was investigated in 1L MoS_2 [28] and also WS_2 [50,55].

The increase of trion contribution at the flake perimeter, observed by Bao et al. [33], suggests an additional *n*-doping of the perimeter compared to the interior. However, nonuniform strain influences the carrier distribution over the 2D flake, inducing a *n*-doping of stretched areas [22,50,51]. Hence, the less strained perimeter of CVD-grown flakes should reveal a *p*-doping (or at least a reduced concentration of electrons as the main carriers) and, in turn, a lower trion contribution to the spectrum, as well as a lower trion binding energy.

Observing the opposite, Bao et al. suggested another explanation for their data, involving an effect of the edge. It is known [32] that there are two types of MoS_2 monolayer morphology energetically stable with, respectively, two edge termination. The flakes having the Mo-terminated edge, so called the Mo-zigzag, may be grown adjacent to ones with the S-zigzag. These kinds of edges may affect the doping of the flake perimeter. When explaining trion enhancement at the perimeter, Bao et al. [33] assumed that the edges of their flakes are Mo-terminated. Such edges are metal-rich and could be the origin of additional equilibrium electrons modifying the perimeter doping. The presence of additional carriers enhances the probability of trion formation under optical excitation and could provide Auger recombination, which is supposed in Ref. [33] as the cause of a lower PL efficiency at the perimeter compared to the interior. On the other hand, the MoS_2 flake edges have a very high level of structural disorder such as variations of the Mo-to-S terminated edges and the zigzag-to-armchair edges [35,59–62]. Moreover, such structural nonuniformities of the edge cause (i) a high compressive and tensile strains with a localization of only few nanometers nearly the edge [60] and (ii) a variety of donor and acceptor defect levels at the edge [34,59,62]. As a result of these edge effects, the nano-Raman spectra are shown to be redshifted or blueshifted depending on the edge type [35]. The PL is always highly quenched by non-radiative recombination at defects near the edge (similar to what we observed, in agreement with Bao et al. [33] and other groups [63,64]). It should be emphasized here that the mentioned edge effects on the Raman and PL were observed only at 10–20 nm at the edge. Moreover, there are no reports about a change in the exciton/trion PL towards the edges in unstrained exfoliated flakes. It is thus reasonable to attribute the shift in PL and Raman spectra, as well as the exciton/trion intensity variations near the perimeter (up to about 1 μm near the edge), to the presence of heterogeneous tensile strain [22,28,50,51,55].

The reduction of the A^- trion contribution and the notably higher A^0 exciton emission at the perimeter is in full agreement with the effect of strain, resulting in a drift of electrons towards the strained interior [22] and, as a consequence, *p*-doping on the less strained perimeter. No effect similar to the trion enhancement at the perimeter found by Bao et al. [33] has been observed in our case. Considering that there is no variation of the exciton/trion PL towards the perimeter in unstrained

exfoliated flakes, we suggest to attribute the Raman and PL change over the flake surface to heterogeneous tensile strain.

5. Conclusions

A single 2L MoS_2 flake CVD-grown on a SiO_2/Si substrate was studied by means of micro-Raman/PL combined spectroscopy, focusing on the surface variation of the exciton and trion PL characteristics. The Raman modes and the PL spectrum in the flake interior were found to be redshifted compared to those at the perimeter. This is in accordance with the presence of tensile strain induced by cooling a flake with thermal expansion higher than that of the substrate material. As a result, the flake interior part is strained, while its perimeter is less strained. Tensile strain causes a narrowing of the bandgap observed by the PL redshift in the flake interior. Meanwhile, at the perimeter, the PL blueshift is determined by not only the strain effect but also the weakening of the trion component, which also leads to a narrowing of the PL spectrum. This is attributed to the strain effect leading to a *p*-doping of the perimeter, meaning a drift of electrons towards the strained interior. Briefly, tensile strain bends downward the conduction band edge of MoS_2, causing the drift of electrons towards the strained region and, in turn, creating there an increased electron density which fosters the creation of a negatively charged trion.

Our findings, together with those reported before, allow to conclude that strain in CVD-grown flakes has a general trend to be weaker at the perimeter, while the heterogeneity of strain is apparently random in different flakes and it can also define the excitonic emission characteristics.

Funding and acknowledgements

This work was supported in part by National Research Foundation of Ukraine (2020.02/0134); Ministry of Education and Science of Ukraine (0122U001954); and Key Research and Development Project of Guangdong Province of China (2020B010169003).

Credit authors

Oleksandr I. Datsenko: Investigation, Data curation, Formal analysis, Writing - Original Draft. Sergii Golovynskyi: Conceptualization, Methodology, Investigation, Formal analysis, Writing - Original Draft. Ana I. Pérez-Jiménez: Methodology, Investigation, Formal analysis. Marc Chaigneau: Methodology. Andrii Golovynskyi: Investigation, Formal analysis. Iuliia Golovynska: Investigation. Victoriya Shevchenko: Formal analysis. Matteo Bosi: Resources, Investigation, Writing - Review & Editing. Luca Seravalli: Investigation, Writing - Review & Editing.

Declaration of competing interest

The authors declare that they have no known competing financial interests or personal relationships that could have appeared to influence the work reported in this paper.

Data availability

Data will be made available on request.

References

[1] A.K. Geim, K.S. Novoselov, The rise of graphene, Nat. Mater. 6 (3) (2007) 183–191.
[2] R. Mas-Ballesté, C. Gómez-Navarro, J. Gómez-Herrero, F. Zamora, 2D materials: to graphene and beyond, Nanoscale 3 (1) (2011) 20–30.
[3] B. Guo, Q.l. Xiao, S.h. Wang, H. Zhang, 2D layered materials: synthesis, nonlinear optical properties, and device applications, Laser Photon. Rev. 13 (12) (2019), 1800327.
[4] S. Golovynskyi, Nanomaterials for optoelectronics: an editor's overview, Ukr. J. Phys. Opt. 24 (5) (2023) S1–S9.
[5] K.F. Mak, C. Lee, J. Hone, J. Shan, T.F. Heinz, Atomically thin MoS_2: a new direct-gap semiconductor, Phys. Rev. Lett. 105 (13) (2010), 136805.
[6] A. Splendiani, L. Sun, Y. Zhang, T. Li, J. Kim, C.-Y. Chim, G. Galli, F. Wang, Emerging photoluminescence in monolayer MoS_2, Nano Lett. 10 (4) (2010) 1271–1275.
[7] K.F. Mak, K. He, C. Lee, G.H. Lee, J. Hone, T.F. Heinz, J. Shan, Tightly bound trions in monolayer MoS_2, Nat. Mater. 12 (3) (2013) 207.
[8] S. Catalán-Gómez, S. Garg, A. Redondo-Cubero, N. Gordillo, A. Andres, F. Nucciarelli, S. Kim, P. Kung, J. Pau, Photoluminescence enhancement of monolayer MoS_2 using plasmonic gallium nanoparticles, Nanoscale Adv. 1 (2019) 884–893.
[9] Z. Luo, H. Jia, L. Lv, Q. Wang, X. Yan, Gate-tunable trion binding energy in monolayer MoS_2 with plasmonic superlattice, Nanoscale 12 (34) (2020) 17754–17761.
[10] I. Irfan, S. Golovynskyi, M. Bosi, L. Seravalli, O.A. Yeshchenko, B. Xue, D. Dong, Y. Lin, R. Qiu, B. Li, J. Qu, Enhancement of Raman scattering and exciton/trion photoluminescence of monolayer and few-layer MoS_2 by Ag nanoprisms and nanoparticles: shape and size effects, J. Phys. Chem. C 125 (7) (2021) 4119–4132.
[11] I. Irfan, S. Golovynskyi, O.A. Yeshchenko, M. Bosi, T. Zhou, B. Xue, B. Li, J. Qu, L. Seravalli, Plasmonic enhancement of exciton and trion photoluminescence in 2D MoS_2 decorated with Au nanorods: impact of nonspherical shape, Physica E 140 (2022), 115213.
[12] F. Prins, A.J. Goodman, W.A. Tisdale, Reduced dielectric screening and enhanced energy transfer in single- and few-layer MoS_2, Nano Lett. 14 (11) (2014) 6087–6091.
[13] D. Prasai, A.R. Klots, A.K.M. Newaz, J.S. Niezgoda, N.J. Orfield, C.A. Escobar, A. Wynn, A. Efimov, G.K. Jennings, S.J. Rosenthal, K.I. Bolotin, Electrical control of near-field energy transfer between quantum dots and two-dimensional semiconductors, Nano Lett. 15 (7) (2015) 4374–4380.
[14] D. Kufer, I. Nikitskiy, T. Lasanta, G. Navickaite, F.H.L. Koppens, G. Konstantatos, Hybrid 2D-0D MoS_2-PbS quantum dot photodetectors, Adv. Mater. 27 (1) (2015) 176–180.
[15] Z. Li, R. Ye, R. Feng, Y. Kang, X. Zhu, J.M. Tour, Z. Fang, Graphene quantum dots doping of MoS_2 monolayers, Adv. Mater. 27 (35) (2015) 5235–5240.
[16] D. Kufer, T. Lasanta, M. Bernechea, F.H.L. Koppens, G. Konstantatos, Interface engineering in hybrid quantum dot–2D phototransistors, ACS Photonics 3 (7) (2016) 1324–1330.
[17] A. Raja, A. Montoya−Castillo, J. Zultak, X.-X. Zhang, Z. Ye, C. Roquelet, D. A. Chenet, A.M. van der Zande, P. Huang, S. Jockusch, J. Hone, D.R. Reichman, L. E. Brus, T.F. Heinz, Energy transfer from quantum dots to graphene and MoS_2: the role of absorption and screening in two-dimensional materials, Nano Lett. 16 (4) (2016) 2328–2333.
[18] M. Li, J.S. Chen, P.K. Routh, P. Zahl, C.Y. Nam, M. Cotlet, Distinct optoelectronic signatures for charge transfer and energy transfer in quantum dot–MoS_2 hybrid photodetectors revealed by photocurrent imaging microscopy, Adv. Funct. Mater. 28 (29) (2018), 1707558.
[19] J.J. Gough, N. McEvoy, M. O'Brien, J. McManus, J. Garcia-Coindreau, A.P. Bell, D. McCloskey, C. Hrelescu, G.S. Duesberg, A.L. Bradley, Dependence of photocurrent enhancements in hybrid quantum dot-MoS_2 devices on quantum dot emission wavelength, ACS Photonics 6 (4) (2019) 976–984.
[20] L.P.L. Mawlong, A. Bora, P.K. Giri, Coupled charge transfer dynamics and photoluminescence quenching in monolayer MoS_2 decorated with WS_2 quantum dots, Sci. Rep. 9 (1) (2019), 19414.
[21] S. Golovynskyi, O.I. Datsenko, D. Dong, Y. Lin, I. Golovynska, Z. Jin, B. Li, H. Wu, MoS_2 monolayer quantum dots on a flake: efficient sensitization of exciton and trion photoluminescence via resonant nonradiative energy and charge transfers, Appl. Surf. Sci. 601 (2022), 154209.
[22] A. Castellanos-Gomez, R. Roldán, E. Cappelluti, M. Buscema, F. Guinea, H.S.J. van der Zant, G.A. Steele, Local strain engineering in atomically thin MoS_2, Nano Lett. 13 (11) (2013) 5361–5366.
[23] H.J. Conley, B. Wang, J.I. Ziegler, R.F. Haglund, S.T. Pantelides, K.I. Bolotin, Bandgap engineering of strained monolayer and bilayer MoS_2, Nano Lett. 13 (8) (2013) 3626–3630.
[24] Y.Y. Hui, X. Liu, W. Jie, N.Y. Chan, J. Hao, Y.-T. Hsu, L.-J. Li, W. Guo, S.P. Lau, Exceptional tunability of band energy in a compressively strained trilayer MoS_2 sheet, ACS Nano 7 (8) (2013) 7126–7131.
[25] Z. Liu, M. Amani, S. Najmaei, Q. Xu, X. Zou, W. Zhou, T. Yu, C. Qiu, A.G. Birdwell, F.J. Crowne, R. Vajtai, B.I. Yakobson, Z. Xia, M. Dubey, P.M. Ajayan, J. Lou, Strain and structure heterogeneity in MoS_2 atomic layers grown by chemical vapour deposition, Nat. Commun. 5 (1) (2014) 5246.
[26] S. Deng, S. Che, R. Debbarma, V. Berry, Strain in a single wrinkle on an MoS_2 flake for in-plane realignment of band structure for enhanced photo-response, Nanoscale 11 (2) (2019) 504–511.
[27] F. Carrascoso, H. Li, R. Frisenda, A. Castellanos-Gomez, Strain engineering in single-, bi- and tri-layer MoS_2, $MoSe_2$, WS_2 and WSe_2, Nano Res. 14 (6) (2020) 1698–1703.
[28] A. Michail, D. Anestopoulos, N. Delikoukos, J. Parthenios, S. Grammatikopoulos, S. A. Tsirkas, N.N. Lathiotakis, O. Frank, K. Filintoglou, K. Papagelis, Biaxial strain engineering of CVD and exfoliated single- and bi-layer MoS_2 crystals, 2D Mater. 8 (1) (2020), 015023.
[29] L. Seravalli, M. Bosi, A review on chemical vapour deposition of two-dimensional MoS_2 flakes, Materials 14 (24) (2021) 7590.
[30] S. Luo, C.P. Cullen, G. Guo, J. Zhong, G.S. Duesberg, Investigation of growth-induced strain in monolayer MoS_2 grown by chemical vapor deposition, Appl. Surf. Sci. 508 (2020), 145126.

[31] S. Golovynskyi, D. Dong, Y. Lin, O.I. Datsenko, B. Li, Hexagram bi-layer MoS_2 flake: the impact of polycrystallinity and strains on the exciton and trion photoluminescence, Surface. Interfac. 26 (2021), 101343.
[32] A.M. van der Zande, P.Y. Huang, D.A. Chenet, T.C. Berkelbach, Y. You, G.-H. Lee, T.F. Heinz, D.R. Reichman, D.A. Muller, J.C. Hone, Grains and grain boundaries in highly crystalline monolayer molybdenum disulphide, Nat. Mater. 12 (6) (2013) 554–561.
[33] W. Bao, N.J. Borys, C. Ko, J. Suh, W. Fan, A. Thron, Y. Zhang, A. Buyanin, J. Zhang, S. Cabrini, P.D. Ashby, A. Weber-Bargioni, S. Tongay, S. Aloni, D.F. Ogletree, J. Wu, M.B. Salmeron, P.J. Schuck, Visualizing nanoscale excitonic relaxation properties of disordered edges and grain boundaries in monolayer molybdenum disulfide, Nat. Commun. 6 (1) (2015) 7993.
[34] D. Wu, X. Li, L. Luan, X. Wu, W. Li, M.N. Yogeesh, R. Ghosh, Z. Chu, D. Akinwande, Q. Niu, K. Lai, Uncovering edge states and electrical inhomogeneity in MoS_2 field-effect transistors, Proc. Natl. Acad. Sci. USA 113 (31) (2016) 8583–8588.
[35] T.-X. Huang, X. Cong, S.-S. Wu, K.-Q. Lin, X. Yao, Y.-H. He, J.-B. Wu, Y.-F. Bao, S.-C. Huang, X. Wang, P.-H. Tan, B. Ren, Probing the edge-related properties of atomically thin MoS_2 at nanoscale, Nat. Commun. 10 (1) (2019) 5544.
[36] J. Pei, J. Yang, R. Xu, Y.-H. Zeng, Y.W. Myint, S. Zhang, J.-C. Zheng, Q. Qin, X. Wang, W. Jiang, Y. Lu, Exciton and trion dynamics in bilayer MoS_2, Small 11 (48) (2015) 6384–6390.
[37] S. Golovynskyi, O.I. Datsenko, D. Dong, Y. Lin, I. Irfan, B. Li, D. Lin, J. Qu, Trion binding energy variation on photoluminescence excitation energy and power during direct to indirect bandgap crossover in monolayer and few-layer MoS_2, J. Phys. Chem. C 125 (32) (2021) 17806–17819.
[38] A. Bablich, D.S. Schneider, P. Kienitz, S. Kataria, S. Wagner, C. Yim, N. McEvoy, O. Engstrom, J. Müller, Y. Sakalli, B. Butz, G.S. Duesberg, P.H. Bolívar, M. C. Lemme, Few-layer MoS_2/a-Si:H heterojunction pin-photodiodes for extended infrared detection, ACS Photonics 6 (6) (2019) 1372–1378.
[39] J. Guo, S. Li, Z. He, Y. Li, Z. Lei, Y. Liu, W. Huang, T. Gong, Q. Ai, L. Mao, Y. He, Y. Ke, S. Zhou, B. Yu, Near-infrared photodetector based on few-layer MoS_2 with sensitivity enhanced by localized surface plasmon resonance, Appl. Surf. Sci. 483 (2019) 1037–1043.
[40] D. Maeso, A. Castellanos-Gomez, N. Agraït, G. Rubio-Bollinger, Fast yet quantum-efficient few-layer vertical MoS_2 photodetectors, Adv. Electron. Mater. 5 (7) (2019), 1900141.
[41] J. Ren, B. Guo, Y. Feng, K. Yu, Few-layer MoS_2 dendrites as a highly active humidity sensor, Physica E 116 (2020), 113782.
[42] S. Golovynskyi, I. Irfan, M. Bosi, L. Seravalli, O.I. Datsenko, I. Golovynska, B. Li, D. Lin, J. Qu, Exciton and trion in few-layer MoS_2: thickness- and temperature-dependent photoluminescence, Appl. Surf. Sci. 515 (2020), 146033.
[43] A.R. Rezk, B. Carey, A.F. Chrimes, D.W. Lau, B.C. Gibson, C. Zheng, M.S. Fuhrer, L. Y. Yeo, K. Kalantar-zadeh, Acoustically-driven trion and exciton modulation in piezoelectric two-dimensional MoS_2, Nano Lett. 16 (2) (2016) 849–855.
[44] E. Rotunno, M. Bosi, L. Seravalli, G. Salviati, F. Fabbri, Influence of organic promoter gradient on the MoS_2 growth dynamics, Nanoscale Adv. 2 (6) (2020) 2352–2362.
[45] L. Seravalli, M. Bosi, P. Fiorenza, S.E. Panasci, D. Orsi, E. Rotunno, L. Cristofolini, F. Rossi, F. Giannazzo, F. Fabbri, Gold nanoparticle assisted synthesis of MoS_2 monolayers by chemical vapor deposition, Nanoscale Adv. 3 (16) (2021) 4826–4833.
[46] S. Mouri, Y. Miyauchi, K. Matsuda, Tunable photoluminescence of monolayer MoS_2 via chemical doping, Nano Lett. 13 (12) (2013) 5944–5948.
[47] Y.A. Romaniuk, S. Golovynskyi, A.P. Litvinchuk, D. Dong, Y. Lin, O.I. Datsenko, M. Bosi, L. Seravalli, I.S. Babichuk, V.O. Yukhymchuk, B. Li, J. Qu, Influence of anharmonicity and interlayer interaction on Raman spectra in mono- and few-layer MoS_2: a computational study, Physica E 136 (2021) 114999.
[48] J.G. Kim, W.S. Yun, S. Jo, J. Lee, C.-H. Cho, Effect of interlayer interactions on exciton luminescence in atomic-layered MoS_2 crystals, Sci. Rep. 6 (1) (2016), 29813.
[49] S. Kondratenko, O.I. Datsenko, D. Babich, V. Dzhagan, Y. Pan, M. Rahaman, O. Selyshchev, D.R.T. Zahn, Enhanced photoconductivity of hybrid 2D-QD MoS_2–$AgInS_2$ structures, J. Chem. Phys. 159 (4) (2023), 044707.
[50] M.G. Harats, J.N. Kirchhof, M. Qiao, K. Greben, K.I. Bolotin, Dynamics and efficient conversion of excitons to trions in non-uniformly strained monolayer WS_2, Nat. Photonics 14 (5) (2020) 324–329.
[51] R. Frisenda, A. Castellanos-Gomez, Strain creates a trion factory, Nat. Photonics 14 (5) (2020) 269–270.
[52] J. Xiang, R.N. Ali, Y. Yang, Z. Zheng, B. Xiang, X. Cui, Monolayer MoS_2 thermoelectric properties engineering via strain effect, Physica E 109 (2019) 248–252.
[53] X. He, H. Li, Z. Zhu, Z. Dai, Y. Yang, P. Yang, Q. Zhang, P. Li, U. Schwingenschlogl, X. Zhang, Strain engineering in monolayer WS_2, MoS_2, and the WS_2/MoS_2 heterostructure, Appl. Phys. Lett. 109 (17) (2016), 173105.
[54] W. Deng, X. Chen, Y. Li, C. You, F. Chu, S. Li, B. An, Y. Ma, L. Liao, Y. Zhang, Strain effect enhanced ultrasensitive MoS_2 nanoscroll avalanche photodetector, J. Phys. Chem. Lett. 11 (11) (2020) 4490–4497.
[55] Y. Wang, C. Cong, W. Yang, J. Shang, N. Peimyoo, Y. Chen, J. Kang, J. Wang, W. Huang, T. Yu, Strain-induced direct–indirect bandgap transition and phonon modulation in monolayer WS_2, Nano Res. 8 (8) (2015) 2562–2572.
[56] R.A. Suris, V.P. Kochereshko, G.V. Astakhov, D.R. Yakovlev, W. Ossau, J. Nurnberger, W. Faschinger, G. Landwehr, T. Wojtowicz, G. Karczewski, J. Kossut, Excitons and trions modified by interaction with a two-dimensional electron gas, Phys. Status Solidi 227 (2) (2001) 343–352.
[57] D.K. Efimkin, A.H. MacDonald, Many-body theory of trion absorption features in two-dimensional semiconductors, Phys. Rev. B 95 (3) (2017), 035417.
[58] K.K. Madapu, S. Dhara, Laser-induced anharmonicity vs thermally induced biaxial compressive strain in mono- and bilayer MoS_2 grown via CVD, AIP Adv. 10 (8) (2020), 085003.
[59] W. Zhou, X. Zou, S. Najmaei, Z. Liu, Y. Shi, J. Kong, J. Lou, P.M. Ajayan, B. I. Yakobson, J.-C. Idrobo, Intrinsic structural defects in monolayer molybdenum disulfide, Nano Lett. 13 (6) (2013) 2615–2622.
[60] M. Tinoco, L. Maduro, M. Masaki, E. Okunishi, S. Conesa-Boj, Strain-dependent edge structures in MoS_2 layers, Nano Lett. 17 (11) (2017) 7021–7026.
[61] N. Salazar, S. Rangarajan, J. Rodríguez-Fernández, M. Mavrikakis, J.V. Lauritsen, Site-dependent reactivity of MoS_2 nanoparticles in hydrodesulfurization of thiophene, Nat. Commun. 11 (1) (2020) 4369.
[62] J. Dong, D. Ding, C. Jin, Y. Liu, F. Ding, Edge reconstruction-dependent growth kinetics of MoS_2, ACS Nano 17 (1) (2022) 127–136.
[63] Y. Okuno, O. Lancry, A. Tempez, C. Cairone, M. Bosi, F. Fabbri, M. Chaigneau, Probing the nanoscale light emission properties of a CVD-grown MoS_2 monolayer by tip-enhanced photoluminescence, Nanoscale 10 (29) (2018) 14055–14059.
[64] A. Rodriguez, M. Kalbáč, O. Frank, Strong localization effects in the photoluminescence of transition metal dichalcogenide heterobilayers, 2D Mater. 8 (2) (2021), 025028.